

Analyzing powers A_{yy} , A_{xx} , A_{xz} and A_y in the $dd \rightarrow {}^3\text{He}n$ reaction at 270 MeV

M. Janek^{1,2a}, T. Saito³, V.P. Ladygin^{1b}, T. Uesaka^{4c}, M. Hatano³, A.Yu. Isupov¹, H. Kato³, N.B. Ladygina¹, Y. Maeda⁴, A.I. Malakhov¹, J. Nishikawa⁵, T. Ohnishi⁶, H. Okamura⁷, S.G. Reznikov¹, H. Sakai^{3,4}, S. Sakoda³, N. Sakamoto⁶, Y. Satou⁸, K. Sekiguchi⁶, K. Suda⁴, A. Tamii⁸, N. Uchigashima³, T.A. Vasiliev¹, and K. Yako³

¹ VBLHE-JINR, 141980 Dubna, Moscow region, Russia

² University of P.J. Šafárik, 041-54 Košice, Slovakia

³ Department of Physics, University of Tokyo, Bunkyo, Tokyo 113-0033, Japan

⁴ Center for Nuclear Study, University of Tokyo, Bunkyo, Tokyo 113-0033, Japan

⁵ Department of Physics, Saitama University, Urawa 338-8570, Japan

⁶ RIKEN, Wako, Saitama 351-0198, Japan

⁷ CYRIC, Tohoku University, Sendai, Miyagi 980-8578, Japan

⁸ Research Center for Nuclear Physics, Osaka University, Ibaraki 567-0047, Japan

Received: date / Revised version: date

Abstract. The data on the tensor A_{yy} , A_{xx} , A_{xz} and vector A_y analyzing powers in the $dd \rightarrow {}^3\text{He}n$ obtained at $T_d = 270$ MeV in the angular range $0^\circ - 110^\circ$ in the c.m. are presented. The observed negative sign of the tensor analyzing powers A_{yy} , A_{xx} and A_{xz} at small angles clearly demonstrate the sensitivity to the ratio of the D and S wave component of the ${}^3\text{He}$ wave function. However, the one-nucleon exchange calculations by using the standard ${}^3\text{He}$ wave functions have failed to reproduce the strong variation of the tensor analyzing powers as a function of the angle in the c.m.

PACS. 24.70.+s Polarization phenomena in reactions – 25.10.+s Nuclear reactions involving few-nucleon system – 21.45.+v Few-body systems

1 Introduction

Intensive theoretical and experimental efforts performed during last years led to a new generation of realistic nucleon-nucleon (NN) potentials like AV-18 [1], CD-Bonn [2], Nijmegen I, II and 93 [3] etc. These potentials describe the existing NN scattering data up to 350 MeV with an unprecedented precision. However, already in the elastic Nd scattering there are significant discrepancies between the measured observables and the Faddeev calculations based on pairwise NN potentials (see review [4] and references therein). A part of this discrepancy in the cross section at the energies ≤ 135 MeV/nucleon [5,6] has been reduced by including three nucleon forces ($3NF$). At higher kinetic energies, the backward angles require more sophisticated approaches with a new type of $3NF$ and/or relativistic corrections [6,7]. On the other hand, Faddeev calculations cannot reproduce the behavior of the polarization observables in the dp elastic scattering [7,8,9,10,11,12,13]. These results clearly indicate deficiencies in the spin-

dependent part of the $3NF$ models used in the calculations.

In this respect, three nucleon bound states are of particular interest, because even such a fundamental quantity as the binding energy of the system cannot be reproduced by calculations with modern pairwise nucleon-nucleon potentials [4]. Since the binding energy is known to be closely related with the power of spin-dependent forces such as the tensor and/or three-nucleon forces, an experimental study of the spin structure of three-nucleon bound system is crucial to understand the source of underbinding.

The non-relativistic Faddeev calculations [14] for three-nucleon bound state have predicted that the dominant components of the ${}^3\text{He}$ ground state are as follows: a spatially symmetric S -state, where the ${}^3\text{He}$ spin due to the neutron and two protons are in a spin singlet state; and a D -state, where all three nucleon spins are oriented opposite to the ${}^3\text{He}$ spin. The S -state is found to dominate at small momenta while D -state dominates at large momenta. The relative sign of the D - and S -waves in the momentum space is positive at small and moderate nucleon momenta [15]. The data sensitive to the three-nucleon bound state spin structure are scarce and new polarization data, especially at short internucleonic distances, are of great importance.

^a E-mail address: janek@sunhe.jinr.ru

^b E-mail address: ladygin@sunhe.jinr.ru

^c E-mail address: uesaka@cns.s.u-tokyo.ac.jp

The ${}^3\text{He}$ structure information is contained in the spin-dependent spectral function $S_{\hat{\sigma}}^N(E, \mathbf{q})$ [16], defined as the probability density of nucleon N found in the ${}^3\text{He}$ nucleus with separation energy E , momentum \mathbf{q} , and spin along (opposite to) the ${}^3\text{He}$ spin indicated by $\hat{\sigma}=+(-)$. The nucleon momentum distribution in ${}^3\text{He}$ is described by the spin-averaged spectral function $S^N(E, \mathbf{q})$.

The nucleon momentum distribution, or $S^N(E, \mathbf{q})$, was investigated by the reactions of quasielastic knockout of the ${}^3\text{He}$ constituent nucleons. The spectral functions $S^N(E, \mathbf{q})$ extracted by the plane-wave impulse approximation (PWIA) analysis from the ${}^3\text{He}(e, ep)$ [17], ${}^3\text{He}(p, 2p)d$, and ${}^3\text{He}(p, pd)p$ reactions [18], were found to be in a reasonable agreement.

To investigate the spin-dependent spectral function $S_{\hat{\sigma}}^N(E, \mathbf{q})$, one needs to measure the polarization observables. Spin correlations for the quasielastic ${}^3\text{He}(p, pN)$ reactions were measured at IUCF Cooler Ring [19] up to the internal nucleon momentum $q \sim 400$ MeV/ c . The spin asymmetry in the momentum distribution proportional to $S_+^N(E, \mathbf{q}) - S_-^N(E, \mathbf{q})$, was extracted from the experimental results by the PWIA analysis and compared with the Faddeev solution. A good agreement of the experimental neutron and proton spin-dependent spectral functions with the Faddeev calculations [14] was observed at low nucleon momenta. However, there is a discrepancy between the experiment and theory in the region of $q \geq 300$ MeV/ c . This deviation can be caused by the uncertainty of the high-momentum spin structure of the ${}^3\text{He}$ as well as by the reaction mechanisms which have not been taken into account in PWIA.

The radiative deuteron-proton capture reaction, $dp \rightarrow {}^3\text{He}\gamma$, at intermediate energies involves a large momentum transfer and therefore can be used to study high momentum components of the ${}^3\text{He}$ wave function. The measurements of the tensor analyzing powers [20] have shown their sensitivity to the D -state component in ${}^3\text{He}$. Recently the vector A_y and tensor A_{yy} , A_{xx} analyzing powers have been measured at *KVI* at 55, 66.5 and 90 MeV/nucleon [21]. The data are in a good agreement with the results of Faddeev calculations obtained by the Bochum-Cracow [22] and Hannover groups [23], which have shown the effect of $3NF$ to be small at these energies. However, the *KVI* data [21] are in strong contradiction with the A_{xx} data obtained at 100 MeV/nucleon at *RCNP* [24].

The $d{}^3\text{He}$ - backward elastic scattering and $dd \rightarrow {}^3\text{He}n({}^3\text{He}p)$ reactions at intermediate and high energies are the one-nucleon exchange (ONE) processes with a large momentum transfer and, therefore, can be used as an effective tool to investigate the ${}^3\text{He}$ structure at short distances. The theoretical analysis of the $dd \rightarrow {}^3\text{He}n$ reaction [25] performed within ONE approximation, has shown that the tensor analyzing powers due to polarization of the incident deuteron are sensitive to the spin distribution of neutron, when ${}^3\text{He}$ is emitted in the forward direction in the c.m. Tensor analyzing powers are sensitive to the ratio of the D and S wave component of the ${}^3\text{He}$ wave function at intermediate energies [25, 26].

The polarization data for dd - scattering at intermediate energies are scarce. But more data have been obtained on the analyzing powers in the dd - elastic scattering [27], $dd \rightarrow {}^3\text{He}n$ and $dd \rightarrow {}^3\text{He}p$ reactions [28] at low energies. These data have been reproduced with the four-body calculations by solving Alt-Grassberger-Sandhas [29] and Faddeev-Yakubovsky [30] equations, and hyperspherical harmonics methods [31]. However, at the moment these calculations cannot be applied to the higher energies.

The experiment on the measurement of the energy and angular dependences of the tensor analyzing powers in the $dd \rightarrow {}^3\text{He}n({}^3\text{He}p)$ process in the conditions, when the contribution from the D - state in ${}^3\text{He}({}^3\text{H})$ becomes larger, has been performed at RIKEN. Obtained at the deuteron kinetic energy of 140, 200 and 270 MeV the data on the tensor analyzing powers T_{20} in the $dd \rightarrow {}^3\text{He}(0^\circ)n({}^3\text{H}(0^\circ)p)$ reaction have positive values [32], which are in a good agreement with the T_{20} data in $d{}^3\text{He}$ - backward elastic scattering [33] and clearly demonstrate the sensitivity to the D - wave effect in the three nucleon bound states.

This paper gives the data on the angular distribution of the analyzing powers A_{yy} , A_{xx} , A_{xz} and A_y in the $dd \rightarrow {}^3\text{He}n$ reaction at 270 MeV of the deuteron kinetic energy. The details of the experimental procedure are described in section 2, the results are discussed in section 3, the conclusions are written in section 4.

2 Experiment

The experiment has been performed at RIKEN Accelerator Research Facility. The details of the experiment were discussed elsewhere [32], below we mention briefly the main items of the experimental procedure.

The high-intensity polarized deuteron beam was produced by the polarized ion source (PIS) [34] and accelerated by the AVF and Ring Cyclotrons up to the energy of 270 MeV. The direction of the symmetry axis of the beam polarization was controlled with a Wien-filter located at the exit of the PIS.

The polarization of the deuteron beam was measured with two beam-line polarimeters. The dp elastic scattering was used with the known large values of the tensor and vector analyzing powers A_y , A_{yy} , A_{xx} and A_{xz} [8, 9]. These data of the analyzing powers [8, 9] were taken to analyze dp - elastic scattering at 140 and 270 MeV. The values were obtained for the polarized deuteron beam, whose absolute polarization had been calibrated via the ${}^{12}\text{C}(d, \alpha){}^{10}\text{B}^*[2^+]$ reaction [35].

The first polarimeter situated downstream of the Ring Cyclotron was used for the beam polarization monitoring while taking data. The second polarimeter (*SWPOL*) located in front of the scattering chamber in the experimental hall measured polarization before and after each run. The polarization values obtained from the both polarimeters agreed with each other within the statistical accuracy, therefore, the beam polarization for each polarization state of the PIS was taken as a weighted average of the values obtained by these polarimeters.

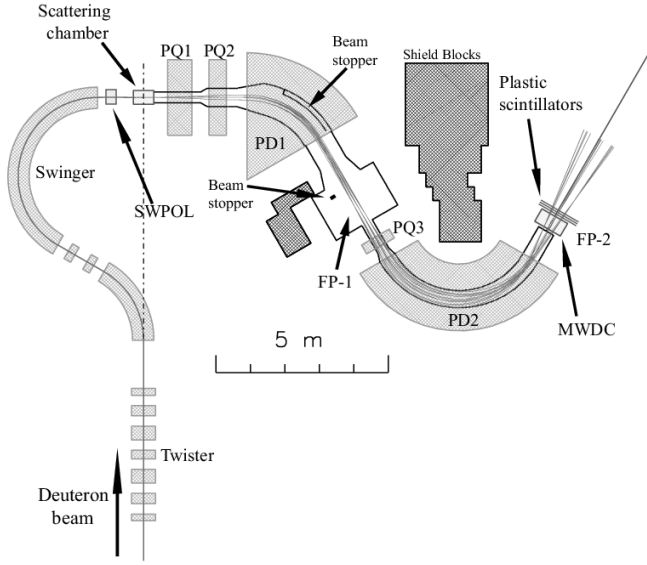


Fig. 1. Spectrometer SMART and the detection system. PD_i and PQ_i are the dipole and quadrupole magnets, respectively; $MWDC$ are the multiwire drift chambers; $SWPOL$ is the beam-line deuteron polarimeter; $FP1$ and $FP2$ are the focal planes of the spectrometer.

In the present experiment the data were taken for the vector and tensor polarization modes which had the following theoretical maximum polarization: $(p_z, p_{zz}) = (0, 0), (0, -2), (-2/3, 0)$ and $(1/3, 1)$. The actual values of the beam polarization were between 45 and 85 % of the maximum theoretical value. The systematic error due to the uncertainties of the dp -elastic scattering analyzing power values [8,9] does not exceed $\sim 2\%$ both for the vector and tensor polarization of the beam. The systematic and statistical errors have been added in quadrature to calculate the total error of the beam polarization values.

The layout of the experiment is shown in Fig.1. SMART spectrograph (Swinger and Magnetic Analyzer with a Rotator and a Twister) [36] was used for these measurements. The measurements of the particle momentum and separation from the primary beam were performed by the magnetic system of SMART spectrograph consisting of two dipole and three quadrupole magnets (Q-Q-D-Q-D).

Two deuterated polyethylene (CD_2) sheets of 54 mg/cm^2 and 32 mg/cm^2 thick [37] placed in the scattering chamber of the SMART were taken as the deuterium targets. The carbon foil 34 mg/cm^2 thick was used to measure the background spectra.

The detection system of SMART at the focal point $FP2$ consisted of three plastic scintillation counters and a multiwire drift chamber (MWDC). The coincidence of the signal outputs of all the three scintillation counters was employed as the event trigger. Pulse heights of the plastic scintillation counters were used to select the particle of interest at the trigger level. Protons and deuterons were partly suppressed by raising threshold levels of the constant fraction discriminators. The fraction of the event rate for single-charged particles was $\sim 40\%$. The CFD

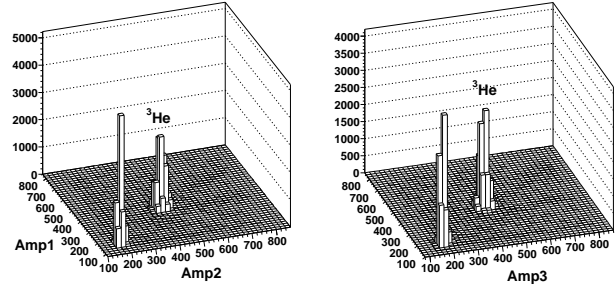


Fig. 2. Correlation of the amplitudes in the scintillation detectors. The left (right) panel corresponds to the correlation for the 1st and 2nd (the 1st and 3rd) counters.

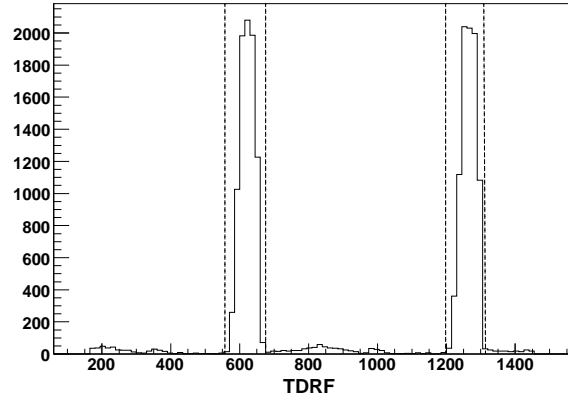


Fig. 3. The time difference between the trigger signal and the radio-frequency signal of the cyclotron. The dashed lines represent the imposed windows to select the ${}^3\text{He}$ nuclei.

thresholds were tuned in such a way not to lose the ${}^3\text{He}$ events keeping the dead-time of the data acquisition system at the level of 20-30%. The admixtures of the background events were almost completely eliminated by a software cut in the offline analysis.

The particle identification was carried out on the energy losses in the plastic scintillators and time-of-flight between the target and the detection point. The event was considered as a certain type of particle (${}^3\text{He}$) only in the case when the pulse height was correlated in all three scintillation counters. The correlation of the amplitudes in the 1st and 2nd (the 1st and 3rd) scintillation detectors is presented in the left (right) panel of Fig.2. The distance between the target and the detection point was about 17 m, which was enough to separate ${}^3\text{He}$, deuterons, and protons with the same momentum from the time-of-flight (TOF - the time difference between the trigger signal and the radio-frequency signal of the cyclotron, see Fig.3). The start signal to measure TOF came from the event trigger. The imposed windows to select the ${}^3\text{He}$ nuclei are shown in Fig.3 by the dashed lines.

The MWDC information was taken to reconstruct the particle trajectories in the focal plane $FP2$. The trajectories of the detected particles at the second focal plane were determined by the least square method using the position

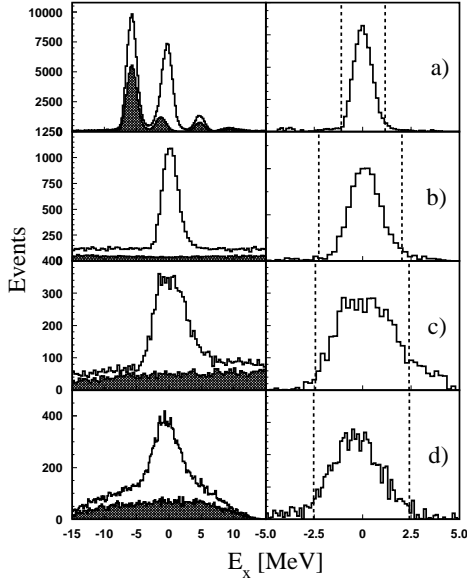


Fig. 4. $\text{CD}_2\text{-C}$ subtraction for the $dd \rightarrow {}^3\text{He}n$ reaction at $T_d = 270$ MeV. The open and shadowed histograms in the left panels correspond to the yields from the CD_2 and carbon targets, respectively. The right panels demonstrate the quality of the $\text{CD}_2\text{-C}$ subtraction. The panels a), b), c) and d) correspond to the ${}^3\text{He}$ scattering angle in the c.m. of 5° , 32° , 54° and 94° , respectively.

information obtained from the MWDC. The typical track reconstruction efficiency of the MWDC was better than 99%. The ion-optical parameters of the SMART spectrograph were also taken into account to calculate the momentum of the particle and emission angle in the target to obtain the track information. The resulting energy resolution was ~ 300 keV.

The contribution of the deuterium target was obtained via $\text{CD}_2\text{-C}$ subtraction procedure for each spin state at every angle. Subtraction procedure is shown in Fig.4 a), b), c) and d) for the ${}^3\text{He}$ scattering angle in the c.m. of 5° , 32° , 54° and 94° , respectively. The spectra are plotted as a function of the excitation energy E_X defined as follows:

$$E_X = \sqrt{(E_0 - E_{3N})^2 - (\mathbf{P}_0 - \mathbf{P}_{3N})^2} - M_N, \quad (1)$$

where \mathbf{P}_0 is the incident momentum; $E_0 = 2M_d + T_d$ is the total initial energy; E_{3N} and \mathbf{P}_{3N} are the energy and momentum of the three-nucleon system, respectively; M_N is the nucleon mass. The left panels represent the relative yields from the CD_2 and carbon targets shown by the open and shadowed histograms, respectively. The histograms are not normalized for the sake of easy comparison. Peaks at $E_X = 0$ MeV correspond to ${}^3\text{He}$ from the $dd \rightarrow {}^3\text{He}n$ reaction. The right panels show the spectra after subtraction of the carbon events normalized on luminosity and dead-time correction. It is clearly demonstrated that the subtraction procedure has been carried out properly.

The analyzing powers A_y , A_{yy} , A_{xx} and A_{xz} in the $dd \rightarrow {}^3\text{He}n$ reaction were obtained from the number of

Table 1. The angular dependence of the vector analyzing power A_y in the $dd \rightarrow {}^3\text{He}n$ reaction at 270 MeV.

$\theta_{c.m.}$	$A_y \pm \Delta A_y$	$\theta_{c.m.}$	$A_y \pm \Delta A_y$
1.0	-0.012 ± 0.026	54.0	-0.393 ± 0.029
3.0	-0.037 ± 0.016	56.0	-0.326 ± 0.032
5.0	-0.019 ± 0.014	58.0	-0.274 ± 0.024
7.0	-0.081 ± 0.012	60.0	-0.327 ± 0.029
10.0	-0.098 ± 0.012	62.0	-0.348 ± 0.024
12.0	-0.136 ± 0.013	64.0	-0.266 ± 0.024
14.0	-0.133 ± 0.015	66.0	-0.348 ± 0.024
16.0	-0.146 ± 0.016	68.0	-0.326 ± 0.025
18.0	-0.129 ± 0.018	70.0	-0.299 ± 0.024
20.0	-0.119 ± 0.022	72.0	-0.331 ± 0.026
22.0	-0.085 ± 0.024	74.0	-0.271 ± 0.024
24.0	-0.075 ± 0.031	76.0	-0.323 ± 0.027
26.0	-0.018 ± 0.016	78.0	-0.333 ± 0.037
28.0	-0.026 ± 0.012	80.0	-0.290 ± 0.035
30.0	-0.023 ± 0.012	82.0	-0.351 ± 0.033
32.0	-0.043 ± 0.012	84.0	-0.310 ± 0.025
34.0	-0.040 ± 0.013	86.0	-0.172 ± 0.044
36.0	-0.075 ± 0.015	88.0	-0.251 ± 0.044
38.0	-0.093 ± 0.013	90.0	-0.292 ± 0.030
40.0	-0.153 ± 0.020	92.0	-0.349 ± 0.026
42.0	-0.166 ± 0.027	94.0	-0.310 ± 0.024
44.0	-0.177 ± 0.029	96.0	-0.095 ± 0.058
46.0	-0.194 ± 0.031	98.0	-0.181 ± 0.048
48.0	-0.282 ± 0.024	100.0	-0.116 ± 0.062
50.0	-0.329 ± 0.030	104.0	-0.123 ± 0.054
52.0	-0.331 ± 0.032		

the events after the $\text{CD}_2\text{-C}$ subtraction procedure and beam polarization. The number of the events was normalized on the dead-time effect, the detection efficiency, and beam intensity. When the ${}^3\text{He}$ scattering angle in the c.m. was equal to or less than 7° , the azimuthal angle to cover the scattered particles became larger. In this case the range of the azimuthal angle was divided into bins of 15 degrees. The asymmetry from each bin for each polarized spin mode of PIS was acquired individually and the analyzing powers were obtained from the fit of the asymmetries distribution by the functions depending on the azimuthal angle. Since the polarization modes were cycled every 5 seconds, the systematic uncertainty due to any time-dependent effects such as deuterium loss from the CD_2 target caused by beam irradiation, can be neglected.

3 Results and discussion

The results on the angular distribution of the analyzing powers A_y , A_{yy} , A_{xx} and A_{xz} in the $dd \rightarrow {}^3\text{He}n$ reaction at the incident deuteron energy $T_d = 270$ MeV are given in tables 1, 2, 3 and 4, respectively. The systematic and the statistical error of analyzing powers have been added in quadrature.

The angular dependence of the vector A_y and tensor A_{yy} , A_{xx} and A_{xz} analyzing powers at the energy $T_d = 270$

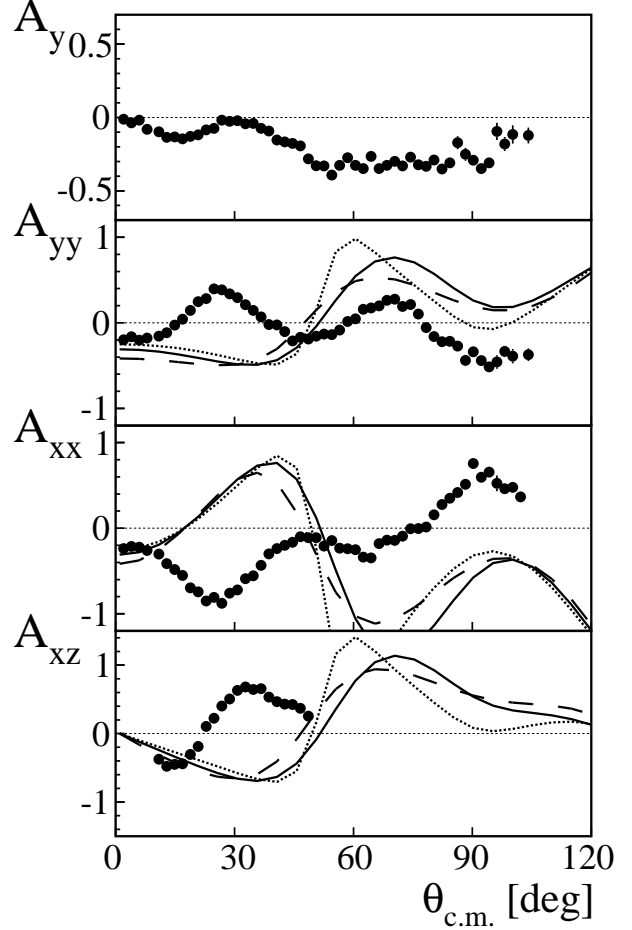
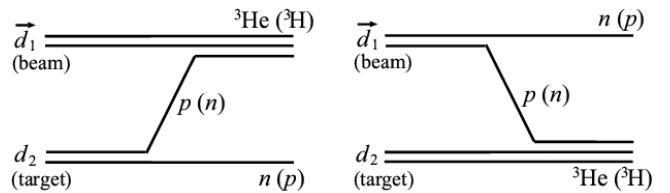
Table 2. The angular dependence of the tensor analyzing power A_{yy} in the $dd \rightarrow {}^3\text{He}n$ reaction at 270 MeV.

$\theta_{c.m.}$	$A_{yy} \pm \Delta A_{yy}$	$\theta_{c.m.}$	$A_{yy} \pm \Delta A_{yy}$
1.0	-0.184 ± 0.027	54.0	-0.139 ± 0.041
3.0	-0.204 ± 0.018	56.0	-0.085 ± 0.044
5.0	-0.209 ± 0.027	58.0	0.015 ± 0.032
7.0	-0.192 ± 0.033	60.0	0.047 ± 0.040
10.0	-0.155 ± 0.017	62.0	0.159 ± 0.031
12.0	-0.116 ± 0.018	64.0	0.173 ± 0.031
14.0	-0.027 ± 0.019	66.0	0.198 ± 0.031
16.0	0.042 ± 0.021	68.0	0.262 ± 0.032
18.0	0.145 ± 0.022	70.0	0.277 ± 0.031
20.0	0.248 ± 0.026	72.0	0.192 ± 0.034
22.0	0.283 ± 0.028	74.0	0.213 ± 0.033
24.0	0.397 ± 0.035	76.0	0.102 ± 0.039
26.0	0.385 ± 0.018	78.0	-0.055 ± 0.055
28.0	0.338 ± 0.013	80.0	-0.160 ± 0.054
30.0	0.294 ± 0.014	82.0	-0.221 ± 0.051
32.0	0.211 ± 0.014	84.0	-0.217 ± 0.037
34.0	0.145 ± 0.015	86.0	-0.272 ± 0.063
36.0	0.070 ± 0.018	88.0	-0.440 ± 0.066
38.0	-0.020 ± 0.017	90.0	-0.339 ± 0.044
40.0	-0.025 ± 0.027	92.0	-0.441 ± 0.038
42.0	-0.102 ± 0.035	94.0	-0.514 ± 0.036
44.0	-0.212 ± 0.041	96.0	-0.457 ± 0.079
46.0	-0.169 ± 0.044	98.0	-0.335 ± 0.066
48.0	-0.189 ± 0.034	100.0	-0.389 ± 0.083
50.0	-0.156 ± 0.041	104.0	-0.372 ± 0.073
52.0	-0.132 ± 0.045		

MeV are presented in Fig.5. The errors of the analyzing powers include both the statistical and systematic errors due to the uncertainty in the beam polarization. One can see strong variations of the analyzing powers as a function of the angle in the c.m.

The negative sign of A_{yy} and A_{xx} values at small scattering angles is in a striking contrast to the positive A_{yy} and A_{xx} for the $dp \rightarrow pd$ [9,38] or $d^3\text{He} \rightarrow p^4\text{He}$ [39] reactions where the deuteron structure is relevant. The negative tensor analyzing powers can be understood in terms of the ratio of the D and S wave component of the ${}^3\text{He}$ wave function by means of ONE calculations.

Within the framework of ONE approximation the $dd \rightarrow {}^3\text{He}n$ process can be described by a sum of 2 diagrams (see Fig.6) required by the symmetry of the initial state of the reaction. If the ${}^3\text{He}$ is scattered at forward angles the contribution of the second diagram becomes negligible due to a large relative momentum between the nucleons in the deuteron. Consequently, only the first diagram gives the contribution to the cross section and polarization observables. It has been found [32] that the tensor analyzing powers due to polarization of the deuteron beam are sensitive to the ratio of the D and S wave component of the ${}^3\text{He}$ and deuteron wave function, when ${}^3\text{He}$ is emitted in the forward and backward directions in the c.m., respectively.

**Fig. 5.** The results on the vector A_y and tensor A_{yy} , A_{xx} and A_{xz} analyzing powers at energy $T_d=270$ MeV as a function of the angle in the c.m. The solid, dashed and dotted curves are the results of the non-relativistic ONE calculations [25,26] using Urbana [40], Paris [41] and RSC [42] ${}^3\text{He}$ wave functions, respectively. Paris deuteron wave function [44] was used to describe the deuteron structure.**Fig. 6.** ONE diagrams for the $dd \rightarrow {}^3\text{He}n$ reaction.

The solid, dashed, and dotted curves in Fig.5 are the results of non-relativistic ONE calculations [25,26] using Urbana [40], Paris [41] and RSC [42] (with the parametrization from [43]) wave functions of ${}^3\text{He}$. The Paris parametrization [44] was applied for the deuteron wave function.

The negative sign of the tensor analyzing powers A_{yy} and A_{xx} at small scattering angles reflects the positive sign of the ratio of the D/S wave component of the ${}^3\text{He}$ wave

Table 3. The angular dependence of the tensor analyzing power A_{xx} in the $dd \rightarrow {}^3\text{He}n$ reaction at 270 MeV.

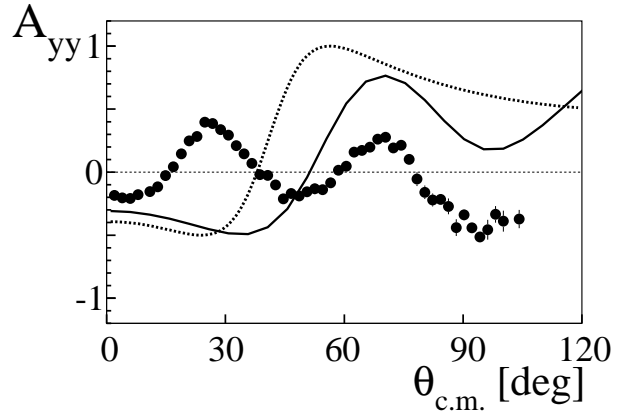
$\theta_{c.m.}$	$A_{xx} \pm \Delta A_{xx}$	$\theta_{c.m.}$	$A_{xx} \pm \Delta A_{xx}$
1.0	-0.237 ± 0.028	54.0	-0.144 ± 0.049
3.0	-0.210 ± 0.017	56.0	-0.233 ± 0.058
5.0	-0.221 ± 0.023	58.0	-0.241 ± 0.047
7.0	-0.260 ± 0.025	60.0	-0.252 ± 0.062
10.0	-0.302 ± 0.041	62.0	-0.338 ± 0.042
12.0	-0.413 ± 0.041	64.0	-0.347 ± 0.043
14.0	-0.482 ± 0.045	66.0	-0.179 ± 0.046
16.0	-0.551 ± 0.007	68.0	-0.139 ± 0.033
18.0	-0.697 ± 0.034	70.0	-0.141 ± 0.026
20.0	-0.744 ± 0.038	72.0	-0.092 ± 0.027
22.0	-0.851 ± 0.038	74.0	-0.006 ± 0.038
24.0	-0.808 ± 0.041	76.0	-0.003 ± 0.053
26.0	-0.877 ± 0.039	78.0	0.013 ± 0.048
28.0	-0.759 ± 0.036	80.0	0.156 ± 0.054
30.0	-0.722 ± 0.038	82.0	0.277 ± 0.043
32.0	-0.589 ± 0.037	84.0	0.351 ± 0.038
34.0	-0.556 ± 0.037	86.0	0.417 ± 0.042
36.0	-0.435 ± 0.039	88.0	0.512 ± 0.046
38.0	-0.301 ± 0.027	90.0	0.755 ± 0.056
40.0	-0.239 ± 0.034	92.0	0.595 ± 0.029
42.0	-0.199 ± 0.036	94.0	0.656 ± 0.043
44.0	-0.165 ± 0.036	96.0	0.524 ± 0.091
46.0	-0.099 ± 0.040	98.0	0.461 ± 0.052
48.0	-0.110 ± 0.044	100.0	0.478 ± 0.039
50.0	-0.112 ± 0.036	102.0	0.365 ± 0.051
52.0	-0.209 ± 0.052		

Table 4. The angular dependence of the tensor analyzing power A_{xz} in the $dd \rightarrow {}^3\text{He}n$ reaction at 270 MeV.

$\theta_{c.m.}$	$A_{xz} \pm \Delta A_{xz}$	$\theta_{c.m.}$	$A_{xz} \pm \Delta A_{xz}$
10.0	-0.374 ± 0.024	30.0	0.630 ± 0.025
12.0	-0.478 ± 0.027	32.0	0.682 ± 0.027
14.0	-0.449 ± 0.031	34.0	0.644 ± 0.030
16.0	-0.442 ± 0.032	36.0	0.657 ± 0.035
18.0	-0.305 ± 0.040	38.0	0.532 ± 0.024
20.0	-0.188 ± 0.034	40.0	0.465 ± 0.032
22.0	0.103 ± 0.037	42.0	0.430 ± 0.035
24.0	0.224 ± 0.041	44.0	0.424 ± 0.036
26.0	0.401 ± 0.046	46.0	0.370 ± 0.044
28.0	0.505 ± 0.051	48.0	0.256 ± 0.059

function in the momentum space. This behaviour of the data is consistent with the D -state admixture in the ${}^3\text{He}$ predicted in several theoretical works [14,15]. However, the trend of the tensor analyzing powers A_{yy} and A_{xx} at the angles below 15° in the c.m. is opposite to the ONE calculations.

The strong disagreement of the experimental data from the non-relativistic ONE calculations [25,26] is observed at angles larger than 15° in the c.m. The discrepancy between the data and the calculations shown in Fig.5 can be explained by the reaction mechanism which differs from

**Fig. 7.** The results on the tensor analyzing power A_{yy} at energy $T_d=270$ MeV as a function of the ${}^3\text{He}$ scattering angle in the c.m. The solid and dashed curves are the results of ONE calculations using non-relativistic and relativistic Urbana [40] ${}^3\text{He}$ wave functions, respectively.

ONE and/or by the non-adequate description of the short-range ${}^3\text{He}$ spin structure. One of the additional mechanisms can be the Δ -isobar excitation. This mechanism has been taken into account phenomenologically to describe the T_{20} data in the $d^3\text{He}$ - backward elastic scattering [33]. The microscopic calculation by Laget et al.[41] has shown that the coherent sum of ONE and the Δ -isobar excitation reasonably reproduces the cross section for the $dd \rightarrow {}^3\text{He}n$ reaction at GeV energies. The calculation predicts that the Δ -isobar contribution to the cross section is 10% at most in the energy region lower than 300 MeV. It is a dominating contribution to the ONE process. On the other hand, our data on the vector analyzing power A_y have values of ~ -0.35 at the angles larger than 50° , while ONE predicts vanishing vector analyzing powers. Thus our data have clearly indicated that the processes which are not included in the calculations in ref.[32] are important in this angular region.

The analysis of the experimental data on the cross sections of the $dp \rightarrow pd$ and $dd \rightarrow {}^3\text{He}n$ reactions [45] has shown that non-nucleonic degrees of freedom can occur already at $T_d \sim 500$ MeV. The large angles in the c.m. in the present experiment correspond to the short internucleonic distances where the manifestation of non-nucleonic degrees of freedom is possible. On the other hand, the discrepancy between the data on the tensor analyzing powers and ONE calculations [25,26] can be caused by the relativistic effects. In Fig.7 the tensor analyzing power A_{yy} in the $dd \rightarrow {}^3\text{He}n$ reaction at 270 MeV is compared with the results of ONE calculations using the relativistic and non-relativistic Urbana ${}^3\text{He}$ wave function [40] shown by the dashed and solid lines, respectively. Relativity in ${}^3\text{He}$ wave function is taken into account by the minimal relativization scheme [46], where a non-relativistic argument of the wave function is replaced by the light-cone variable k (with the corresponding renormalization of the wave function)

[47]:

$$k^2 = \frac{[\alpha^2 m_{dT}^2 - (1 - \alpha)^2 m_{pT}^2]^2}{4\alpha(1 - \alpha)[\alpha m_{dT}^2 + (1 - \alpha)m_{pT}^2]} + p_T^2, \quad (2)$$

$$m_{dT}^2 = m_d^2 + p_T^2, \quad m_{pT}^2 = m_p^2 + p_T^2,$$

where m_d and m_p are the deuteron and proton masses, m_{dT} and m_{pT} are the deuteron and proton transversal masses, α is the longitudinal momentum fraction taken away by the deuteron in the infinite momentum frame, and p_T is the transverse momentum.

One can see that the use of the relativistic ${}^3\text{He}$ wave function [46] does not allow one to reproduce A_{yy} data. The structure of ${}^3\text{He}$ can be more complicated and depends on more than one variable as in the case of the deuteron where the strong dependence of the spin structure on two variables was observed [48]. On the other hand, the relativistic effects for the both reaction mechanisms and ${}^3\text{He}$ structure should be treated in the consistent way. For instance, if one takes the relativistic kinematics, boost effects and Wigner spin rotations, it finally leads to rather small effects in the cross section and polarization observables in Nd -elastic scattering [49].

The observed negative sign of the tensor analyzing powers A_{yy} , A_{xx} and A_{xz} at small angles has demonstrated the sensitivity to the ratio of the D and S wave component of the ${}^3\text{He}$ wave function. However, the deviation of the experimental data from the ONE calculations at large angles can be due to not only the nonadequate description of the short range ${}^3\text{He}$ spin structure, but also to the influence of the mechanisms additional to ONE. The measurements of the polarization observables in the $dd \rightarrow {}^3\text{He}n$ process can provide independent information on the ${}^3\text{He}$ spin structure with respect to the data for the ${}^3\text{He}(p, pN)$ [19] and $dp \rightarrow {}^3\text{He}\gamma$ [21,24] reactions, where the rescattering and meson-exchange current effects play an important role and mask the structure of ${}^3\text{He}$.

4 Conclusions

The high precision data on the A_{yy} , A_{xx} , A_{xz} and A_y analyzing powers in the $dd \rightarrow {}^3\text{He}n$ reaction at the energy 270 MeV have been obtained.

The ONE calculations using the standard ${}^3\text{He}$ wave functions, non-relativistic and relativistic in the minimal scheme [46], have described qualitatively the data on the tensor analyzing powers A_{yy} , A_{xx} and A_{xz} at small angles. But they have failed to reproduce strong variations of the tensor analyzing powers as a function of the angle in the c.m. According to the calculations [41] the $dd \rightarrow {}^3\text{He}n$ reaction is dominated by ONE at these energies. The Δ -isobar contribution is less than 10% at energies lower than 300 MeV [41]. The deviation of the experimental data from the ONE calculations can be explained by the non-adequate description of the short range spin ${}^3\text{He}$ structure, for instance, manifestation of non-nucleonic degrees of freedom within the theoretical model considered here. On the other hand, it is possible that not considered above reaction mechanisms can affect the polarization data.

The observed features and high precision of the obtained data from the present experiment put serious constraints on the models describing the ${}^3\text{He}$ structure. However, additional measurements of the polarization observables in the $dd \rightarrow {}^3\text{He}n$ reaction at different energies as well as further theoretical calculations are required to improve the description of the obtained data. In this respect, our data are important to study the $dd \rightarrow {}^3\text{He}n$ reaction as a probe to explore the short range spin structure of three nucleon bound state.

The authors express their thanks to the staff of RARF having provided excellent conditions for the R308n experiment. Deep recognition and appreciation is expressed to H.Kumasaka, R.Suzuki and R.Taki for their help during the experiment. The Russian part of collaboration thanks the RIKEN Directorate for kind hospitality while their stay in Japan. The investigation has been partly supported by the Grant-in-Aid for Scientific Research (Grant No. 14740151) of the Ministry of Education, Culture, Sports, Science, and Technology of Japan; by the Russian Foundation for Fundamental Research (Grant No. 07-02-00102-a) and by the Grant Agency for Science at the Ministry of Education of the Slovak Republic (Grant No. 1/4010/07).

References

1. R.B. Wiringa, V. G. J. Stoks and R. Schiavilla, Phys.Rev. C **51**, 38 (1995).
2. R. Machleidt, K. Holinde and Ch. Elster, Phys.Rep. **149**, 1 (1987); R. Machleidt, Adv. Nucl. Phys. **19**, 189 (1989);
3. V. G. J. Stoks R. A. M. Klomp, C. P. F. Terheggen and J.J. de Swart, Phys.Rev.C **49**, 2950 (1994).
4. W. Glöckle et al., Phys. Rep. **274**, 107 (1996).
5. K. Sekiguchi et al., Phys.Rev.Lett. **95**, 162301 (2005).
6. K. Ermisch et al., Phys.Rev. C **68**, 051001(R) (2003).
7. K. Hatanaka et al., Phys.Rev. C **66**, 044002 (2002).
8. N. Sakamoto et al., Phys.Lett. B **367**, 60 (1996).
9. K. Sekiguchi et al., Phys.Rev. C **65**, 034003 (2002).
10. E.J. Stephenson et al., Phys.Rev. C **60**, 061001 (1999); R. Bieber et al., Phys.Rev.Lett. **84**, 606 (2000); H. Sakai et al., Phys.Rev.Lett. **84**, 5288 (2000).
11. R.V. Cadman et al., Phys.Rev.Lett. **86**, 967 (2001); B.v. Przewoski et al., Phys.Rev. C **74**, 064003 (2006).
12. K. Sekiguchi et al., Phys.Rev. C **70**, 014001 (2004).
13. K. Ermisch et al., Phys.Rev. C **71**, 064004 (2005).
14. B. Blankleider and R. M. Woloshyn, Phys. Rev. C **29**, 538 (1984); J. L. Fliar, B. F. Gibson, G. L. Payne, A. M. Bernstein and T. E. Chupp, Phys. Rev. C **42**, 2310 (1990); R. W. Schulze and P. U. Sauer, Phys. Rev. C **48**, 38 (1993).
15. A.M. Eiro and F.D. Santos, J.Phys.G: Nucl.Phys. **16**, 1139 (1990).
16. R. G. Milner et al., Phys.Lett. B **379**, 67 (1996).
17. E. Jans et al., Nucl.Phys. A **475**, 687 (1987).
18. M. B. Epstein et al., Phys.Rev. C **32**, 967 (1985).
19. M. A. Miller et al., Phys.Rev.Lett. **74**, 502 (1995).
20. J. Jourdan et al., Phys.Lett. B **162**, 269 (1986); M. C. Vetterli et al., Phys.Rev.Lett. **54**, 1129 (1985); A. Arriaga and F. D. Santos, Phys.Rev. C **29**, 1945 (1984); W.K. Pitts et al., Phys.Rev. C **37**, 1 (1988); H. Anklin et al., Nucl.Phys. A **636**, 189 (1998).

21. A.A. Mehmandoost-Khajeh-Dad et al., Phys.Lett. B **617**, 18 (2005).
22. R. Skibinski et al., Phys.Rev. C **67**, 054001 (2003); J. Golak et al., Phys.Rev. C **62**, 054005 (2000).
23. A. Deltuva et al., Phys. Rev. C **69**, 034004 (2004).
24. T. Yagita et al., Mod.Phys.Lett. A **18**, 322 (2003).
25. V.P. Ladygin and N.B. Ladygina, Phys.Atom.Nucl. 59 (1996) 789; *ibid.* **65**, 1609 (2002); Nuovo Cim. A **112**, 855 (1999).
26. V.P. Ladygin et al., Part.and Nucl.Lett. **3[100]-2000**, 74 (2000).
27. W. Grüebler et al., Nucl.Phys. A **193**, 149 (1972); H.O. Meyer and P. Schiemenz, Nucl.Phys. A **197**, 259 (1972); B.J. Crowe III et al., Phys.Rev. C **61**, 034006 (2000).
28. E.M. Bernstein et al., Nucl.Phys. A **126**, 641 (1969); W. Grüebler et al., Nucl.Phys. A **193**, 129 (1972); L.G. Dries et al., Phys.Lett. B **80**, 176 (1979); V. König et al., Nucl.Phys. A **331**, 1 (1979).
29. A.C. Fonseca, Few-Body Syst.Suppl. **10**, 359 (1999); Phys.Rev.Lett. **83**, 4021 (1999); A. Deltuva and A.C. Fonseca, Phys.Rev. C **75**, 014005 (2007); arXiv: nucl-th/0703066.
30. F. Ciesielski and J. Carbonell, Phys.Rev. C **58**, 58 (1998); R. Lazauskas and J. Carbonell, Few-Body Syst. **34**, 105 (2004); Phys.Rev. C **70**, 044002 (2004); R. Lazauskas et al., *ibid.* **71**, 034004 (2005).
31. M. Viviani, A. Kievsky and S. Rosati, Phys.Rev. C **71**, 024006 (2005); M. Viviani et al., Few-Body Syst. **39**, 159 (2006).
32. V.P. Ladygin et al., Phys. Lett. B **589**, 47 (2004); Phys.Atom.Nucl. **69**, 1271 (2006).
33. M. Tanifuji et al., Phys.Rev.C **61**, 024602 (2000).
34. H. Okamura et al., AIP Conf.Proc. **293**, 84 (1993).
35. K. Suda et al., Nucl.Instrum. Methods in Phys.Res. A, in press.
36. T. Ichihara et al., Nucl. Phys. A **569**, 287c (1994).
37. Y. Maeda, H. Sakai, K. Hatanaka and A. Tamii, Nucl.Instrum. Methods in Phys.Res. A **490**, 518 (2002).
38. V. Punjabi et al., Phys.Lett. B **350**, 178 (1995).
39. T. Uesaka et al., Phys.Lett. B **467**, 199 (1999); Few-Body Systems Suppl. **12**, 497 (2000); Phys.Lett. B **533**, 1 (2002).
40. R. Schiavilla, V.R. Pandharipande, R.B. Wiringa, Nucl.Phys. A **449**, 219 (1986).
41. J.-M. Laget, J.F. Lecomte, F. Lefebvres, Nucl.Phys. A **370**, 479 (1981).
42. F.D. Santos, A.M. Eiro, A. Barosso, Phys.Rev. C **19**, 238 (1979).
43. Yu.N. Uzikov, EChAYa **29**, 1010 (1998).
44. M. Lacombe, B. Loiseau, R. Vinh Mau, J. Cote, P. Pires, R. de Tourreil, Phys.Lett. B **101**, 139 (1981).
45. Yu.N. Uzikov, JETP. Lett. **81**, 3031 (2005).
46. P.A.M. Dirac, Rev.Mod.Phys. **21**, 392 (1949); S. Weinberg, Phys.Rev. **150**, 1313 (1966); L.L. Frankfurt, M.I. Strikman, Phys.Rep. **76**, 215 (1981).
47. L.S. Azhgirey et al., Nucl.Phys. A **528**, 621 (1991).
48. S.V. Afanasiev et al., Phys.Lett. B **434**, 21 (1998); V.P. Ladygin et al., Few-Body Systems **32**, 127 (2002); L.S. Azhgirey et al., Phys.Lett. B **595**, 151 (2004); V.P. Ladygin et al., Phys.Lett. B **629**, 60 (2005).
49. H. Witala, J. Golak, W. Glöckle and H. Kamada, Phys.Rev. C **71**, 054001 (2005).